Developing a Multi-Joint Upper Limb Exoskeleton Robot for Diagnosis, Therapy, and Outcome Evaluation in Neurorehabilitation

Yupeng Ren, *Senior Member, IEEE*, Sang Hoon Kang, *Member, IEEE*, Hyung-Soon Park, *Member, IEEE*, Yi-Ning Wu, and Li-Qun Zhang, *Senior Member, IEEE*

***Abstract*—Arm impairments in patients post stroke involve the shoulder, elbow and wrist simultaneously. It is not very clear how patients develop spasticity and reduced range of motion (ROM) at the multiple joints and the abnormal couplings among the multiple joints and the multiple degrees-of-freedom (DOF) during passive movement. It is also not clear how they lose independent control of individual joints/DOFs and coordination among the joints/DOFs during voluntary movement. An upper limb exoskeleton robot, the IntelliArm, which can control the shoulder, elbow, and wrist, was developed, aiming to support clinicians and patients with the following integrated capabilities: 1) quantitative, objective, and comprehensive multi-joint neuromechanical pre-evaluation capabilities aiding multi-joint/DOF diagnosis for individual patients; 2) strenuous and safe passive stretching of hypertonic/deformed arm for loosening up muscles/joints based on the robot-aided diagnosis; 3) (assistive/resistive) active reaching training after passive stretching for regaining/improving motor control ability; and 4) quantitative, objective, and comprehensive neuromechanical outcome evaluation at the level of individual joints/DOFs, multiple joints, and whole arm. Feasibility of the integrated capabilities was demonstrated through experiments with stroke survivors and healthy subjects.**

***Index Terms*—Neurorehabilitation, rehabilitation robotics, robot-aided diagnosis, robot-assisted therapy.**

I. Introduction

AMONG many types of neurorehabilitation robots, there is a recent trend of highlighting exoskeleton robots [1]–[4], because of the following additional advantages over end-effector (EE) type robots. Owing to the close alignment of anatomical axes of human arm multi-joints with corresponding mechanical axes of the exoskeleton robot, all the human arm joint angles and torques of interest can be directly measured (i.e., statically fully determined) and individually controlled [2] without encountering nonuniqueness of the inverse kinematic solution of the kinematically redundant human arm and computing joint torques from inverse dynamics that may involve gradually increasing numerical error as the calculation progress from distal to proximal joints. Consequently, the relation between the joint angle and torque (i.e., the impedance or stiffness) can be directly computed. Using planar EE type robots, one cannot obtain shoulder, elbow, and wrist angles, torques, and impedances simultaneously without additional joint kinematics measurement [5]–[8]. Besides, range of motion (ROM) with exoskeleton robots might be larger than that with EE type robots [9], [10], which may limit arm ROM to an area in front of the trunk [3].

Diagnosis, physical therapy, and outcome evaluation are important and essential steps of rehabilitation, and are, thus, preferred to be integrated for effective treatment of complex interrelated symptoms following neurological impairments: loss of individual joint control and coordination among joints [11], [12] (called loss of joint individuation or lack of fractionation [13], [14]), stiff muscles or joints, excessive cross-joint and cross degrees-of-freedom (DOF) coupling, and reduced ROM of multiple joints [15].

Thus, on one hand, rehabilitation robot researches focused on various types robot-assisted therapy: passive stretching [16]–[20] to reduce joint/muscle stiffness, excessive cross-joint/DOF coupling, and to increase muscle strength, passive ROM (PROM) and active ROM (AROM) by loosening up joints and muscles that may have shortened muscle fascicles and left-shifted tension-length relationship [21]; and (assistive/resistive) active movement training, on which majority of the researches focused [2]–[4], [10], [22], to recover motor functions.

On the other hand, there is much less research done on robot-aided diagnosis of sophisticated upper limb multi-joint and multi-DOF (MJMD) impairments (e.g., simultaneous diagnosis of shoulder, elbow, and wrist joints involving nonhorizontal planes) associated with passive and active movements in stroke survivors—who often show stereotypical patterns of adducted and internally rotated shoulder, flexed elbow, pronated forearm, flexed wrist, and clenched fist—although existing rehabilitation robots have been used to evaluate motor impairments post stroke and their changes following therapy on a single joint or on the shoulder and elbow in horizontal plane [5]–[9], [17], [23]–[25]. For clinicians, obviously, it is infeasible to diagnose such changes in the many DOFs and joints simultaneously and quantitatively. Thus, to aid clinicians in

Manuscript received December 28, 2011; revised September 30, 2012; accepted October 07, 2012. Date of publication October 19, 2012; date of current version May 04, 2013. This work was supported in part by grants from the NSF and NIDRR. Y. Ren and S. H. Kang contributed equally to this work.

Y. Ren is with the Rehabilitation Institute of Chicago, Chicago, IL 60611 USA, and also with Rehabtek LLC, Wilmette, IL 60091 USA.

S. H. Kang, H.-S. Park, and Y.-N. Wu are with the Rehabilitation Institute of Chicago and Department of Physical Medicine and Rehabilitation, Northwestern University, Chicago, IL 60611 USA (e-mail: sanghoon.kang@northwestern.edu).

L.-Q. Zhang is with the Rehabilitation Institute of Chicago, Chicago, IL 60611 USA, and also with the Departments of Physical Medicine and Rehabilitation, Orthopaedic Surgery, and Biomedical Engineering, Northwestern University, Chicago, IL 60611 USA (e-mail: l-zhang@northwestern.edu).

Digital Object Identifier 10.1109/TNSRE.2012.2225073

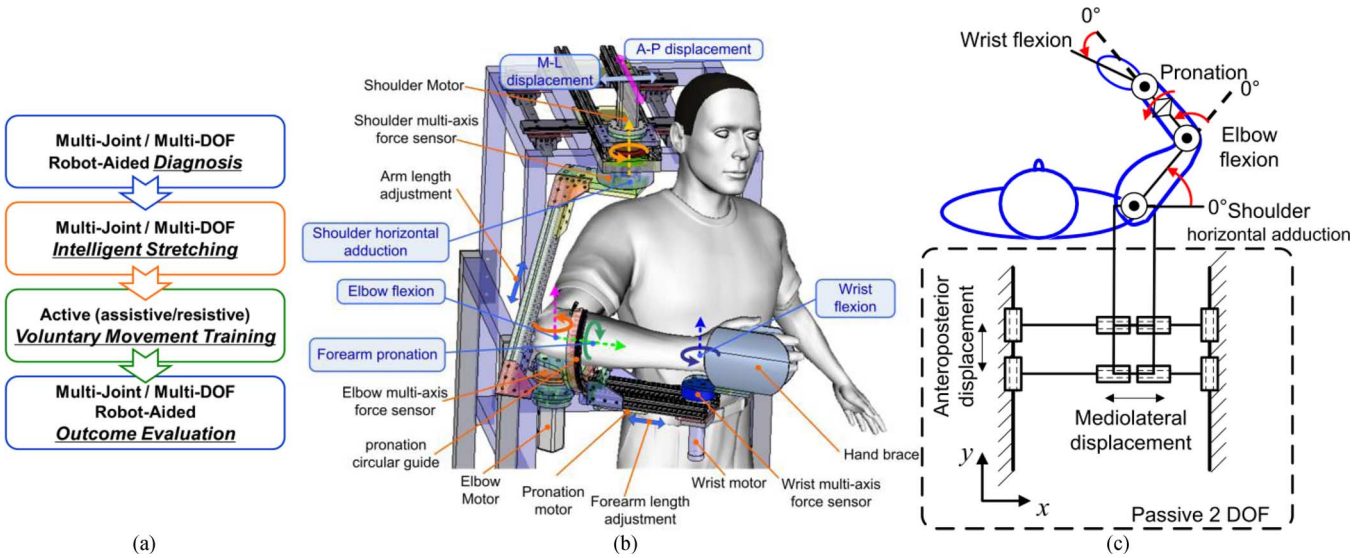

Fig. 1. (a) Four steps essential for the robot-mediated upper limb neurorehabilitation. Diagnosis and outcome evaluation are essential parts of the rehabilitation. Physical therapy can be a combination of passive stretching and active movement training with intensities and durations guided by the clinician's robot-aided diagnosis. (b) Three-dimensional drawing of developed upper limb neurorehabilitation exoskeleton robot, the IntelliArm. (c) Schematic diagram of the IntelliArm (top view in horizontal (transverse) plane). The subject is seated with the upper arm, forearm, and hand attached to the IntelliArm through corresponding rigid braces (not shown in the figure for clarity). Shoulder horizontal adduction, elbow flexion, forearm pronation, wrist flexion were chosen as the positive direction of movement with zero angles defined in Fig. 1(c).

planning therapy by providing MJMD diagnosis of passive/active impairments, a rehabilitation robot with comprehensive measurements of relevant MJMD variables is needed.

Given the complex impairments and symptoms, it may be beneficial for a rehabilitation robot to provide patients a combination of passive stretching and (assistive/resistive) active movement training with intensities and durations of both therapy prescribed by clinicians based on the robot-aided diagnosis for improved outcome [20].

Surprisingly, to the best of authors' knowledge, there is a lack of neurorehabilitation robot reported for aiding all of the aforementioned major steps, although there have been studies addressing utilization of a robot in some parts of neurorehabilitation [1]–[10], [22], [25]–[28].

The purpose of this study was to address the need and develop a 6-DOF upper limb exoskeleton robot, the IntelliArm, aiming to conduct four-step neurorehabilitation with the following integrated capabilities: 1) quantitative, objective, and comprehensive MJMD *pre-evaluation capabilities aiding diagnosis* for individual patients; 2) strenuous and safe *passive stretching* of hypertonic/deformed arm for loosening up muscles/joints based on the robot-aided diagnosis; 3) *active movement training* after the passive stretching for improving motor control ability; and 4) quantitative and comprehensive *outcome evaluation* at the level of individual joints, multiple joints/DOFs, and whole arm. Feasibility of the robot for upper limb MJMD neurorehabilitation was demonstrated through experiments on selected stroke survivors.

II. Methods

A. IntelliArm: An Upper Limb Exoskeleton Robot for Neurorehabilitation

A six-DOF—four active DOFs and two passive DOFs—upper limb neurorehabilitation exoskeleton robot, the IntelliArm, was developed for clinicians to aid MJMD diagnosis and outcome evaluation as well as to assist physical therapy based on the robot-aided diagnosis (Fig. 1).

For pre-evaluation, physical therapy, and outcome evaluation, the subject sat upright comfortably on a sturdy barber's chair. The upper arm, forearm, and hand of the subject were then strapped to the corresponding braces while aligning the subject's shoulder, elbow, and wrist joint axes with the corresponding IntelliArm's mechanical axes [Fig. 1(b) and (c)]. The IntelliArm's elbow and wrist flexion-extension mechanical axes, where the corresponding two servomotors are located, can be adjusted along the upper arm and forearm of the IntelliArm for different human arm lengths.

The IntelliArm can independently control the following four DOFs of human arm: the shoulder horizontal adduction-abduction (H.Add-H.Abd), elbow flexion-extension (Fl-Ex) in horizontal plane, forearm pronation-supination (Pr-Su), and wrist Fl-Ex [Fig. 1(b) and (c)]. For shoulder H.Add-H.Abd, elbow Fl-Ex, and wrist Fl-Ex DOFs, each DOF is driven by a dc motor with a built-in encoder and a zero-backlash harmonic gear (Harmonic Drive) system aligned with the corresponding human arm joint axis.

Since stroke survivors often develop pronation deformity of the forearm, it is important to control and move the forearm in a proper range of pronation. The forearm was mounted to a circular guide through a forearm brace. For the controlled movement of forearm Pr-Su DOF, a dc motor with a built-in encoder (1000 pulse/rev) is used to transmit the power through two stages of transmission: a cable-driven transmission (speed reduction ratio 7:1), output shaft of which is connected to the circular guide by cables, after a precision harmonic gear (50:1, Harmonic Drive) located between the cable-driven transmission and the motor shaft. The maximum output torque and speed of forearm Pr-Su driving system is 10.2 Nm and 49.5°/s, respectively. Since the glenohumeral movement is associated

with scapular movement and stroke survivors often use trunk leaning to compensate for the impaired arm reaching motion, to allow natural arm movement, the robotic arm is mounted on horizontal (transverse) plane frictionless linear guides: one in the anteroposterior (A-P) direction and another in the mediolateral (M-L) directions [Fig. 1(b) and (c)]. The linear guides are also useful for aligning shoulder joint axis with the corresponding IntelliArm joint axis, and can be conveniently locked if needed. The A-P and M-L direction glenohumeral movements were measured by the corresponding direction potentiometers mounted on the linear guides [Fig. 1(b)]. Six-axis force/torque (F/T) sensors [JR3 Inc., Woodland, CA; Fig. 1(b)], located at the shoulder, elbow, and wrist joints, can measure three dimensional forces and torques at those three joints. Due to the hand plate attached after the wrist F/T sensor, the wrist Fl-Ex and forearm Pr-Su direction resistance torque (RT) measurement can be affected by the gravitational torque of the plate. Thus, to subtract the gravitational torque from measured torque, without attaching human arm to the IntelliArm, the gravitational torques about those two axes were measured throughout the whole range of motion of the two DOFs, and the coefficients of the gravitational torque model—a simple multiplication of trigonometric functions of wrist Fl-Ex and forearm Pr-Su angles—were obtained using a standard least square method.

Servo-control and driving of the four DOFs is coordinated by a central digital controller with 0.001 s sampling time. Specifically, for passive mode (i.e., robot drives human arm joints) including the passive stretching, the IntelliArm is position-controlled by receiving the desired velocity generated from the intelligent stretching strategy (ISS) [16], [17], [23] explained in Section II-C; and for active mode (i.e., human arm drives the robot), the IntelliArm is under internal model based impedance control (IMBIC) [29] to make the robot back-drivable. By simply replacing the measured forces and torques with zeros in the IMBIC, position control can be realized with IMBIC. The details of IMBIC can be found in [6]–[8], [29], [30]. Of note is that IMBIC does not require the robot dynamic model or parameters; that it requires small amount of computation, especially in the case of joint space control applications [6]–[8], [29], [30].

During pre-evaluation, physical therapy, and outcome evaluation, for the safety of patients, the joint/DOF angles and RTs are monitored by the central digital controller in real-time, and if either of them is out of its range, the whole IntelliArm system is then shut down in no time. Moreover, mechanical and electrical stops are used to restrict the ROMs of the IntelliArm mechanical axes. Further, a stop switch is given both to the operator and to the subject to authorize them to shut down the IntelliArm system at any time.

The comprehensive MJMD kinetic and kinematic measurements allows us to evaluate the increased stiffness—both individual joint stiffness and cross-coupled stiffness between multi-joints/DOFs—in passive arm movements, and loss of individuation in active arm movement for aiding the diagnosis of the MJMD pathological changes, which may be not easy to be obtained with manual examinations.

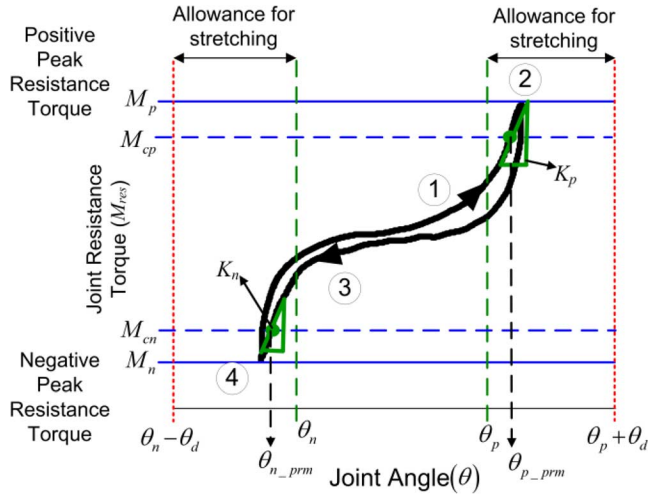

Fig. 2. Typical angle-resistance torque (RT) relationship curve of a joint/DOF. $M_{\rm res}$ denotes joint/DOF RT; M_p and M_n the positive and negative peak RTs, respectively; θ_p and θ_n pre-specified positive and negative end of the PROM, respectively; θ_d the further rotation allowed beyond θ_p and θ_n; M_{cp} and M_{cn} selected positive and negative joint/DOF RTs for obtaining PROM and stiffness of the joint/DOF; θ_{p_prm} and θ_{n_prm} the positive and negative end of PROM at M_{cp} and M_{cn}, respectively; K_p and K_n the joint/DOF stiffness at M_{cp} and M_{cn}, respectively.

The following Sections II-B–II-E describe usage of the IntelliArm in the four-step neurorehabilitation step by step.

B. Multi-Joint Pre-Evaluation of Neuromechanical Changes

The MJMD neuromechanical changes associated with the arm impairment post stroke were characterized systematically by MJMD stiffness—the individual joint stiffness and cross-coupled stiffness between joints/DOFs—during controlled passive movements (i.e., passive mode) and loss of individuation during active movement (i.e., active mode).

1) Multi-Joint/Multi-DOF Passive Changes: The MJMD stiffness as well as PROM and coupled torque (CT) were determined with the IntelliArm operating in the passive mode. Subjects were instructed to relax their arm.

To minimize reflex contributions and manifest the passive mechanical changes of muscles/joints [16], [23], the IntelliArm passively moved one targeted joint/DOF at a time (Fig. 2) among the four controlled DOFs of the subject's arm throughout its ROM with a controlled slow speed (e.g., 10°/s) about five cycles, until its joint/DOF RT, $M_{\rm res}$, reached its pre-specified positive peak RT (PRT), M_p, or negative PRT, M_n, (paths 1 and 3 in Fig. 2); and if $M_{\rm res}$ reached either M_p or M_n, then the movement direction was reversed after few seconds (<10 s) of holding of the joint/DOF at the position where $M_{\rm res}$ is equal to M_p or M_n (point 2 and 4 in Fig. 2, respectively). During this individual joint/DOF movement, all other nontargeted joints/DOFs were immobilized at their selected initial positions, and the torques and angles at all four joints/DOFs were recorded simultaneously.

First, PROM of the targeted joint/DOF was determined from the measured $M_{\rm res}$ and angle, θ, of the targeted joint/DOF. Because the hysteresis loop consist of two paths (one for each direction movement) as observed in the angle-RT ($\theta - M_{\rm res}$)

curves (Fig. 2), positive and negative ends of PROM were defined as follows: positive end of the PROM (θ_{p_prm} in Fig. 2) is the angle where $M_{\rm res}$ is equal to the selected positive joint/DOF RT, M_{cp}, obtained when the joint/DOF is being moved in the positive direction (path 1 in Fig. 2); negative end of the PROM (θ_{n_prm} in Fig. 2) is the angle where $M_{\rm res}$ is equal to the selected negative joint/DOF RT, M_{cn}, obtained when the joint/DOF is being moved in the negative direction (path 3 in Fig. 2). M_{cp} and M_{cn} were slightly smaller than the corresponding direction PRTs in magnitude.

For each joint/DOF, individual joint/DOF stiffness at θ_{p_prm} and θ_{n_prm} (K_p and K_n, respectively, in Fig. 2) was then derived by computing slopes of the $\theta - M_{\rm res}$ curve to represent stiffness at both extreme of PROM. Similarly, from the curves of the angle of targeted joint/DOF versus the CT measured at immobilized joints/DOFs, the cross-coupled stiffness values between the joints/DOFs at θ_{p_prm} and θ_{n_prm} were determined by calculating slopes of each curve. To compute the individual joint/DOF stiffness and cross-coupled stiffness, each of the measured angle-RT (or CT) curves was fitted to a smooth exponential type function shown below, which has been used for passive angle-RT curve fitting of trapeziometacarpal [31], hip [32], [33], knee [33], and ankle [33], [34]

$$M_{{\rm res}\_ij} = a_{1ij} + a_{2ij} e^{a_{3ij}[\theta_j - \max(\theta_j)]} - a_{4ij} \times e^{a_{5ij}[\theta_j - \max(\theta_j)]} \quad (1)$$

where $M_{{\rm res}\_ij}$ denotes ith joint/DOF RT (or CT) induced by the targeted (passively-moved) jth joint/DOF passive movement; θ_j the jth joint/DOF angle; a_{kij} $(k = 1, 2, \ldots, 5)$ constants needed to be determined by the nonlinear least square curve fitting (e.g., the MATLAB function lsqcurvefit). After obtaining a_{kij}, by taking the derivative of (1) with respect to θ_j (i.e., $\partial M_{{\rm res}\_ij}/\partial\theta_j$), stiffness was computed. Since the angle-RT (or CT) curves displayed hysteresis, two exponential type functions were used for fitting one angle-RT (or CT) curve (i.e., one for each path of the hysteresis loop).

The procedure, which could provide complete characterization of all individual joints/DOFs stiffness and cross-coupled stiffness between all joints/DOFs of interest, was repeated for each of the joints/DOFs.

Note that because the PROMs and stiffness—both individual joint and cross-coupled stiffness—were determined at the same joint/DOF RTs (i.e., at M_{cp} and M_{cn}) of the targeted (passively-moved) joint/DOF, fair comparisons of healthy controls and stroke survivors and of the training effect are possible in a quantitative, objective and consistent manner.

2) Multi-Joint/Multi-DOF Active Changes: The loss of individuation was determined with the IntelliArm operating in the active mode. In this mode, subjects can move their arm voluntarily while the arm is strapped to the IntelliArm, because the IntelliArm was made back-drivable under IMBIC [29] with low desired robot impedance (inertia-damping-stiffness): (0.11 Kg·m^2, 0.34 Nm·s/rad, 0 Nm/rad) for shoulder H.Add-H.Abd, (0.11 Kg·m^2, 0.23 Nm·s/rad, 0 Nm/rad) for elbow Fl-Ex, (0.29 Kg·m^2, 0.86 Nm·s/rad, 0 Nm/rad) for forearm Pr-Su, and (0.0034 Kg·m^2, 0.01 Nm·s/rad, 0 Nm/rad) for wrist Fl-Ex.

The active movement evaluation was performed at both the individual joint/DOF and multi-joint levels.

At individual joint/DOF level, individuation in general and loss of individuation post stroke in particular was evaluated. For the quantification of individuation, subjects were instructed to voluntarily move only the targeted joint/DOF without moving all other nontargeted joints/DOFs about 2–5 times with rest between movements to prevent fatigue. Thus, quantification of individuation was possible in two ways: coupled movements (CM) at nontargeted joints/DOFs while the nontargeted joints/DOFs were free to move, and CTs at nontargeted joints/DOFs while the nontargeted joints were immobilized at their initial positions.

To quantify loss of individuation with the measured CMs (i.e., angles) at all other nontargeted joints during targeted joint/DOF voluntary movement, the normalized-root-mean-square-deviation (NRMSD) was computed as

$$d_{{\rm NRMS}\_i,j} = \sqrt{\sum_{k=1}^{N} (\theta_i(k) - \theta_{i\_{\rm init}})^2 N^{-1}} / [\max(\theta_j) - \min(\theta_j)] \quad (2)$$

where $d_{{\rm NRMS}\_i,j}$ denotes the NRMSD; θ_i and θ_j the nontargeted ith joint/DOF angle and the targeted (voluntarily moved) jth joint/DOF angle, respectively; $\theta_{i\_{\rm init}}$ initial angle of the ith joint/DOF; N the number of data points collected. By this way, the nontargeted (and possibly coupled) joint/DOF angle root-mean-square-deviation (RMSD) from its initial angle [numerator of right-hand-side of (2)] can be normalized by the ROM of the targeted (voluntarily moved) joint/DOF [denominator of right-hand-side of (2)]. Thus, with $d_{{\rm NRMS}\_i,j}$, RMSD of nontargeted (ith) joint/DOF angle (θ_i) from its initial angle $(\theta_{i\_{\rm init}})$ induced by the unit targeted (jth) joint/DOF angle (θ_j) change can be quantified. Smaller NRMDS means better individuation.

On the other hand, the CTs at nontargeted (immobilized) joints/DOFs measured during the targeted joint/DOF voluntary movement provided another characterization of individuation.

At the multi-joint level, the hand reaching AROM was determined as the subject was asked to move the hand as far and as wide as possible with all joints/DOFs of the IntelliArm in active (back-drivable) mode.

C. Strenuous and Safe Multi-Joint Intelligent Stretching

Movement and control of the shoulder, elbow, and wrist joints are closely coupled, because of dozens of muscles and other soft tissues crossing the three joints, and some crossing multiple joints. Further, the couplings may increase considerably in hypertonic and deformed arms of patients post stroke. Thus, for effective treatment of hypertonic arms with excessive couplings, the shoulder, elbow, and wrist should be treated together in a well-coordinated manner.

From the robot-aided multi-joint pre-evaluation aiding diagnosis in Section II-B, the joints/DOFs with increased individual joint/DOF stiffness, excessive cross-coupled stiffness, large CTs, and the associated arm postures were identified. The IntelliArm then stretched either multiple joints/DOFs simultaneously or a joint/DOF individually in a *strenuous* and *safe* manner by using the ISS (Fig. 2) [16], [17], [19], [20], [23] to

reduce increased stiffness values and CTs of the joints/DOFs involved. The fingers are not directly stretched, however, because of the possible coupling between the fingers and other joints (e.g., elbow and wrist), fingers might be also stretched during elbow or wrist stretching.

1) Individual Joints Intelligent Stretching: Individual joints/DOFs evaluated as stiff were stretched by the IntelliArm with the ISS [1], [16], [17], [19], [20], [23] to ensure reaching of the extreme ROM pre-specified with manual stretching [θ_p or θ_n in Fig. 2] of the joint/DOF safely by adjusting stretching velocity [$V\ (t)$] based on the RT [$M_{\rm res}\ (t)$] of the joint/DOF with monitoring of the angle [$\theta(t)$] of the joint/DOF. Basically, during stretching (intervals 1 and 3 of Fig. 2), in real-time, $V\ (t)$ was adjusted inversely proportional to $M_{\rm res}\ (t)$ within the maximum $(V_{\max})$ and minimum $(V_{\min})$ magnitude limits (i.e., $V_{\max} \geq |V\ (t)\ | \geq V_{\min} > 0$), until the $M_{\rm res}\ (t)$ reaches pre-specified PRT (i.e., M_p or M_n in Fig. 2). Once the joint/DOF $M_{\rm res}$ reached its PRT, to expect the stress relaxation, the IntelliArm held the joint/DOF at the corresponding position (points 2 and 4 in Fig. 2) for a specified period of time (e.g., 10 s) as used by a therapist. For safety, if the joint angle θ reached $\theta_p + \theta_d$ or $\theta_n - \theta_d$ $(\theta_d > 0)$ then, regardless of the $M_{\rm res}, V(t)$ was set to zero and the joint/DOF stretched was held at that point. Here, θ_d (e.g., 5°) denotes allowed further rotation for effective stretching (Fig. 2). Both position limits (θ_p, θ_n, and θ_d) and PRTs (M_p and M_n) could be set by the operator and were monitored during the passive stretching. In this way, stretching of the muscle-tendons involved, which likely resulted in increased ROM [35], were performed *strenuously* and *safely*.

2) Coordinated Multiple Joints/Multi-DOFs Stretching: Because the arm deformity is characterized with adducted/internally-rotated shoulder, flexed elbow and wrist, and pronated forearm, and hypertonia might exist in both extension and flexion ends of the joints/DOFs, for the MJMD stretching, among many possible multi-joint stretching rules, the following rules were selected [Fig. 3(a)]. Starting at an initial position in the middle of ROMs [points 1 and 5 in Fig. 3(a)], the IntelliArm stretched the four controlled joints/DOFs simultaneously [interval 2 in Fig. 3(a)] to an overall whole-arm extended extreme position [point 3 in Fig. 3(a)]—horizontally abducted shoulder, extended elbow and wrist, and supinated forearm—until the joints/DOFs reached their specified PRTs with stretching velocity generated by the ISS. Once a joint/DOF reached its PRT (or prespecified position limit), it was held at the position until all other joints/DOFs reached their PRTs (or position limit). If the magnitude of RT at the first joint(s)/DOF(s), having reached its PRT, exceeded that of its PRT by more than the pre-specified threshold value (e.g., 1 Nm) due to potential coupling with other joints/DOFs that being stretched to reach their PRT (or position limit), the first joint(s)/DOF(s) was moved back a bit until its RT was back to the PRT. If not, the first joint(s)/DOF(s) was held at the same position. To let the stress relaxation occurs and the stiff joints/DOFs become compliant, after all the joints/DOFs reached the extended extreme position [point 3 in Fig. 3(a)], the arm was held at the posture for a period of time (e.g., 10 s). After the holding, the arm was stretched towards the whole-arm curled extreme position [point 7 in Fig. 3(a)]—horizontally adducted shoulder, flexed elbow and wrist and pronated forearm—in a similar manner.

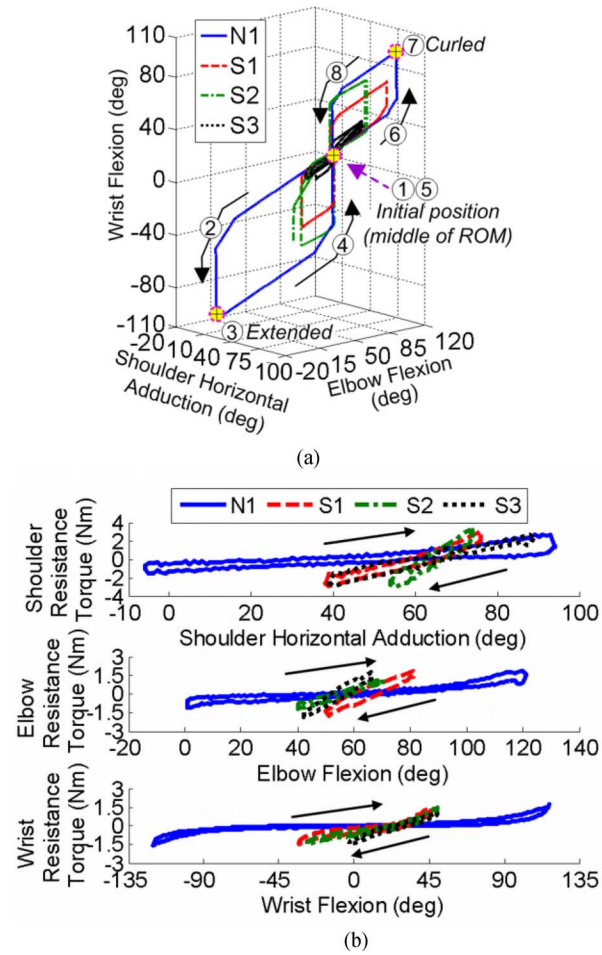

Fig. 3. Passive stretching curves of one healthy control (N1), and three stroke survivors (S1, S2, S3). (a) Shoulder, elbow, and wrist angles during multi-joint passive stretching between the positive and negative PRTs (shoulder: ±3 Nm; Elbow: ±2.5 Nm; Wrist: ±2 Nm); each number in the circle represents the sequence of multi-joint stretching. (b) From the top to the bottom plot, joint angle-RT curves of shoulder, elbow, and wrist, respectively, during each individual joint stretching within the positive and negative PRTs (shoulder: ±2.5 Nm; Elbow: ±1.8 Nm; Wrist: ±1.5 Nm). Arrows represent direction of stretching: sequence of stretching is the same as Fig. 2. The initial joint positions were 70° in shoulder horizontal adduction, 60° elbow flexion and 25° wrist flexion. Compared with the healthy control (N1; blue solid line), stroke survivors demonstrated reduced passive range of motion [(a) and (b)], and increased individual joint stiffness (i.e., slope of the joint angle-RT curve) of shoulder, elbow, and wrist as shown in (b) (see Tables I and II).

D. Multi-Joint Active Movement Training

Motor impairment is associated with both neural and peripheral biomechanical changes. After the controlled stretching reduced the excessive individual joint/DOF stiffness and cross-coupled stiffness, the neural command might be able to control the muscles better and also to move the arm better.

During the (assistive/resistive) active movement training, the IntelliArm was made back-drivable under the IMBIC [6]–[8], [29], [30]. Subjects, thus, were able to move their arm freely

with the IntelliArm to match or track targets displayed on a monitor. To motivate and engage the patients in motor relearning, subjects played computer games.

From the workspace in horizontal (transverse) plane determined by robot-aided diagnosis for an individual subject, a number of target points and desired arm postures in the workspace were displayed. Subjects were asked to move the hand from the current position (displayed as a hatched circle on the screen) to the target (represented as a star), while trying to match the individual joint angles as well. Once a target was reached, it became the new starting position, and a new target in the workspace was displayed for the next move. If the subject could not finish the voluntary movement, assistance would be provided by the IntelliArm to keep the subject engaged. On the other hand, if the subject can perform the movement task easily, resistance could be added to the movement by the IntelliArm to strengthen the impaired arm and to further improve the motor control ability.

E. Multiple Joint Robot-Aided Outcome Evaluations

Similar to the pre-evaluation aiding diagnosis in Section II-B, outcome evaluation was performed in terms of the biomechanical properties and motor-control ability induced by the passive stretching and (assistive/resistive) active movement training at the multiple joints involved.

In the passive mode, the shoulder, elbow, and wrist of the impaired arm of patients were moved by the IntelliArm throughout the ROMs individually or simultaneously under precise control. In the active mode, the patients were asked to move one of the impaired joints/DOFs at a time and to move the multiple joints of the whole-arm simultaneously for functional movements (e.g., reaching).

The MJMD neuromechanical changes in the impaired arm after treatments were evaluated using the data collected from the MJMD passive and active movements. The specific measures include the PROM and the individual joint/DOF stiffness of all joints/DOFs of interest, cross-coupled stiffness between the joints/DOFs, maximum passive CTs, and loss of individuation characterizing active CM/CT, and hand reaching workspace.

III. Experiments

Feasibility of the IntelliArm's integrated capabilities in the four-step neurorehabilitation—pre-evaluation aiding diagnosis, passive stretching, active movement training, and outcome evaluation—were examined by experiments on five subjects.

A. Subjects

Three stroke survivors (age: 52.7 ± 14.7 years; since stroke: 9 ± 2.9 years; sex: 1 F/2M; paralyzed arm: three right-side), numbered as S1, S2, and S3, and two healthy control subjects (age: 31 ± 1 years; sex: 2M; dominant arm: two right-side), numbered as N1 and N2, were recruited for this study, with motor status score (MSS) [36] obtained from the three stroke survivors: MSS of shoulder and elbow of S1, S2, and S3 was 12.32, 5.97, and 8.65, respectively; MSS of wrist, hand, and finger of the three stroke survivors was 0. The two healthy control subjects had no record of previous neurological impairment and musculoskeletal injury/disorder. The study was approved by the institutional review board of Northwestern University. A written consent was obtained from each participant.

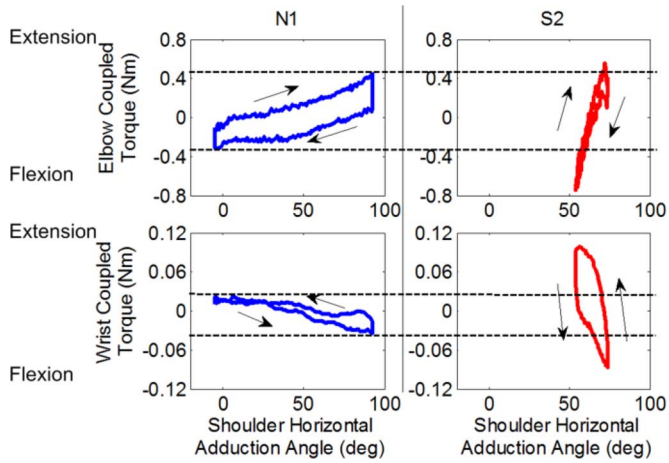

Fig. 4. Shoulder H.Add angle versus elbow and wrist CTs during passive constant slow speed shoulder H.Add-H.Abd movement, shown in first row of Fig. 3(b). Elbow (first row) and wrist (second row) joint CTs measured from a healthy subject (N1, left column) and a stroke survivor (S2, right column) with considerable arm hypertonia/deformity are shown, respectively.

TABLE I
Passive Range of Motion (PROM) of Five Subjects (Mean (Std))

Joint		Passive Range of Motion (deg)			
		Controls	Stroke survivors		
			Before	After	Mean Increase
Shoulder	H. Add	85.9(5.7)	76.9(6.6)	83.4(7.7)	6.5
	H. Abd	-10.2(4.1)	52.6(5.5)	53.2(5.2)	-0.6
Elbow	Fl	97.9(19.6)	72.7(5.9)	82.2(4.7)	9.5
	Ex	0.9 (0.2)	49.8(5.8)	44.1(2.3)	5.7
Wrist	Fl	86.2(13.6)	41.7(3.2)	46.1(9.0)	4.4
	Ex	-88.2(17.7)	-4.2(11.8)	-8.2(12.5)	4.0

PROM of shoulder, elbow and wrist of stroke survivors are reduced compared with those of healthy control subjects at the same torque level. After about 40 minutes stretching, almost all joint PROMs of stroke survivors increased in the sense of mean (last column).

B. Multi-Joint Pre-Evaluation of Neuromechanical Changes

MJMD data of the subjects' arm, obtained with the IntelliArm, were analyzed to aid clinician's diagnosis of the MJMD neuromechanical changes in the impaired arm of patients post stroke, both during passive movements driven by the IntelliArm and during active movements driven by the subjects.

1) Multi-Joint/Multi-DOF Passive Changes: By examining the joint/DOF angle-RT (or CT) torque curves (Figs. 3 and 4) obtained from the passive slow constant speed (10°/s) individual joint/DOF movement between its PRTs, the followings were derived: PROMs (Table I), individual joint/DOF stiffness (Table II), cross-coupled stiffness between joints/DOFs (Table III), and maximum passive CTs. The PRTs were set to be ± 2.5 Nm for shoulder H.Add-H.Abd, ± 1.8 Nm for elbow Fl-Ex, and ± 1.5 Nm for wrist Fl-Ex. Again note that, to minimize the reflex component, each joint/DOF was moved at slow speed, and the subjects were instructed to relax their (impaired) arm.

For objective and consistent comparisons, PROMs and stiffness—both individual joint/DOF stiffness and cross-coupled

TABLE II
INDIVIDUAL JOINT/DOF STIFFNESS AT PROMS IN TABLE I (MEAN (STD))

Joint		Stiffness (Nm/rad)			
		Controls	Stroke survivors		
			Before[a]	After[b]	Mean Change
Shoulder	H.Add	3.91(0.68)	11.56(4.07)	10.63(3.48)	-0.93
	H.Abd	6.02(2.85)	8.90(4.34)	7.05(2.34)	-1.85
Elbow	Fl.	4.83(1.36)	6.63(3.90)	5.98(1.34)	-0.65
	Ex.	2.73(0.03)	6.22(1.98)	5.26(1.34)	-0.96
Wrist	Fl.	1.47(0.14)	3.62(0.32)	3.00(0.32)	-0.62
	Ex.	1.65(0.30)	1.86(0.92)	1.65 (0.71)	-0.21

[a] Before stretching; [b] After 40 min. stretching. Stiffness of all joints/DOFs of stroke survivors is larger than those of healthy controls. After 40 minutes passive stretching, stiffness of all joints/DOFs of stroke survivors were reduced in the sense of mean (last column).

TABLE III
CROSS-COUPLED STIFFNESS MAGNITUDE AT SHOULDER PROMS GIVEN IN TABLE I (MEAN (STD))

Joint	Shoulder PROM	Cross-coupled Stiffness (Nm/rad)			
		Controls	Stroke survivors		
			Before	After	Mean Change
Elbow	H.Add	0.59(0.08)	1.46(0.76)	0.74(0.83)	-0.72
	H.Abd	1.23(1.18)	2.45(0.68)	2.22(0.62)	-0.23
Wrist	H.Add	0.03(0.01)	0.26(0.03)	0.24(0.11)	-0.02
	H.Abd	0.07(0.01)	0.10(0.04)	0.10(0.06)	0.00

Cross-coupled stiffness relating elbow and wrist coupled torques and shoulder H.Add-H.Abd angle were computed using the individual shoulder joint passive stretching data. Compared with the cross-coupled stiffness of healthy controls, those of stroke survivors were large in magnitude. After 40 min. stretching, almost all coupled stiffness – except the wrist coupled stiffness induced by shoulder horizontal abduction – of stroke survivors were reduced in the sense of mean (last column).

stiffness—were obtained at the same RT levels (M_{cp} and M_{cn} in Fig. 2) of each targeted (passively moved) joint/DOF. M_{cp} and M_{cn} pairs of shoulder H.Add-H.Abd, elbow Fl-Ex, and wrist Fl-Ex were set to be (2.5, -1.9) Nm, (1.6, -1.2) Nm, and (0.9, -0.9) Nm, respectively.

Clearly, PROM of all three joints—shoulder, elbow, and wrist—of stroke survivors' spastic and impaired arms were much reduced compared to that of the healthy controls (Table I).

There was relatively less PROM reduction in shoulder H.Add, whereas PROM reductions in shoulder H.Abd, elbow Ex, and wrist Fl and Ex were rather severe.

As was mentioned in Section II-B1), the MJMD stiffness values were obtained by computing slopes of angle-RT (or CT) curves at M_{cp} and M_{cn} of the targeted (passively moved) joint/DOF. The exponential type functions in (1) well accounted for the variance of the data (variance-accounted-for of fitted curves: $97.2 \pm 5.2\%$). Standard deviation of stiffness values of a healthy subject (N2) from five repeated measurements was $5.6 \pm 5.0\%$ of mean stiffness values, thereby showing reliability of the measurements.

Both individual joint/DOF (Table II) and cross-coupled stiffness (Table III) of the stroke survivors were higher than those of healthy controls.

Moreover, we also obtained the CTs at the elbow and at the wrist induced by the individual shoulder passive H.Add-H.Abd movement between shoulder PRTs. During the passive shoulder H.Add, elbow Ex, and wrist Fl CTs were observed; similarly,

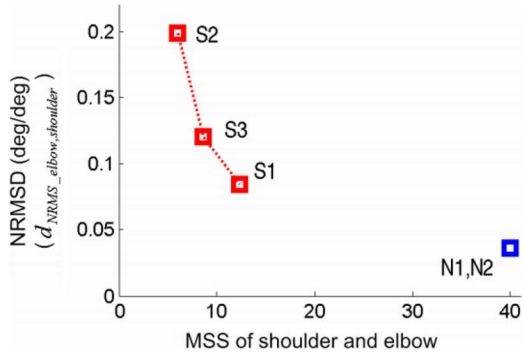

Fig. 5. MSS of shoulder and elbow versus NRMSD of elbow angle induced by the shoulder voluntary horizontal adduction-abduction (H.Add-H.Abd). Two healthy subjects (N1 and N2; blue squares) showed very small and almost indistinguishable NRMSD (0.0366 ± 0.0002) in contrast to that of stroke survivors (0.1349 ± 0.0479; red squares), indicating increased loss of individuation of stroke survivors. Initial angles of shoulder H.Add-H.Abd and elbow Fl-Ex were 70° and 60°, respectively. There may be a potential correlation between NRMSD and MSS of shoulder and elbow, an existing clinical measure: NRMSD of stroke survivors were approximately inversely proportional to MSS of shoulder and elbow of them.

during H.Abd, elbow Fl, and wrist Ex CTs were observed (Fig. 4). The maximum elbow Fl CT of stroke survivors (Ex: 0.57 ± 0.15 Nm; Fl: 1.37 ± 0.19 Nm) were much larger than that (Ex: 0.57 ± 0.01 Nm; Fl: 0.59 ± 0.16 Nm) of the healthy subjects. Maximum wrist CT of stroke survivors (Ex: 0.08 ± 0.02 Nm, Fl: 0.08 ± 0.02 Nm) were also larger than that of healthy controls (Ex: 0.06 ± 0.03 Nm; Fl: 0.05 ± 0.01 Nm). It is probably related to the stiff muscles crossing the joints. Wrist CTs, however, small in magnitude (<0.08 Nm even for stroke survivors), might not be clinically significant.

2) Multi-Joint/Multi-DOF Active Changes: Loss of individuation of the impaired arm during voluntary movement was evaluated. As was discussed in Section II-B2), the loss of individuation may be quantified in two ways: CMs at nontargeted joints/DOFs induced by targeted joint/DOF active movement; and CTs at nontargeted (immobilized) joints/DOFs induced by targeted joint/DOF active movement.

For the CM based quantification of loss of individuation, all joints of the IntelliArm were made to be back-drivable so that the subjects' movement of shoulder H.Add-H.Abd, elbow Fl-Ex, and wrist Fl-Ex were not interfered by the IntelliArm. The subjects were instructed only move one joint/DOF while keeping the initial position of all other joints/DOFs. Stroke survivors showed larger coupled elbow Fl-Ex during active shoulder H.Add-H.Abd than that of healthy controls. As shown in Fig. 5, elbow NRMSD—computed with the elbow Fl-Ex angle (the nontargeted and possibly coupled joint/DOF angle) and the shoulder H.Add-H.Abd angle (the targeted joint/DOF angle)—of stroke survivors (0.1349 ± 0.0479) were much larger than that of healthy controls (0.0366 ± 0.0002). Moreover, the NRMSDs of stroke survivors (S1, S2, and S3) were approximately inversely proportional to the shoulder and elbow MSS scores of them (Fig. 5). Thus, the NRMSD might be useful in quantifying loss of individuation. The CM based quantification of loss of individuation may be further corroborated by CT based quantification.

For CT based quantification of loss of individuation, only one joint of the IntelliArm, corresponding to the targeted joint/DOF

of human arm, was made back-drivable with immobilization of all other joints/DOFs at their initial positions so that only the targeted joint/DOF movement of the subjects' (impaired) arm was allowed. The subjects were instructed to only move the targeted joint/DOF while keeping the initial position of all other nontargeted joints/DOFs.

When the subjects were horizontally adducting-abducting their shoulder while elbow and wrist were immobilized by the IntelliArm, elbow Fl CT of stroke survivors (max. 9.16 ± 3.21 Nm) was considerably larger than that of healthy controls (max. 1.55 ± 0.70 Nm), and was proportionally increasing with increasing shoulder H.Abd angle. This corroborated the loss of individuation quantified by elbow Fl CM, proportionally increasing with increasing shoulder H.Abd angle.

During passive shoulder H.Abd, stroke survivors also generated elbow Fl CT (Fig. 4). However, the elbow Fl CT during active shoulder H.Abd (max. 8.90 ± 3.26 Nm) was much higher than that during passive shoulder H.Abd (max. 1.37 ± 0.19 Nm). This may indicate that the abnormal coactivation of the elbow flexors, including biceps, was a more significant factor contributing to the elbow CT/CM than the passive stiffness of the elbow flexors during shoulder active H.Abd.

Abnormal couplings of distal joints can be similarly analyzed. When the subjects were asked to only flex-extend the wrist without moving other joints/DOFs while all other joints were fixed by the IntelliArm, the healthy subjects flex-extend their wrist with negligible elbow Fl CT (max. 0.075 ± 0.31 Nm), whereas the patients with mild impairment generated substantial elbow Fl CT (S1: max. 15.52 Nm, S2: max. 13.88 Nm), and the patient with severe impairment (S3) could not move the wrist and generated relatively small elbow torque (max. 3.04 Nm) through its coupling with the shoulder. Similarly, when the subjects were asked to pronate-supinate the forearm without moving other joints/DOFs while all other joints/DOFs were fixed by the IntelliArm, the healthy subjects could pronate-supinate their forearm with negligible elbow CT (max. 0.59 ± 0.45 Nm), whereas, the patients with mild impairment generated substantial elbow Fl CT (S1: max. 15.39 Nm, S2: max. 8.98 Nm). For the patient with severe impairment (S3), it was almost impossible to control the forearm Pr-Su movement (range of motion: $40° - 48°$ pronation; max. elbow Fl CT: 1.14 Nm). The limited reaching workspace of the stroke survivors [Fig. 6(a)] could be analyzed further at the individual joint/DOF level [Fig. 6(b)–(d)] for better understanding of the reduced workspace and potentially guiding therapy. Patients with different degrees of impairment showed different amount of workspace reduction [Fig. 6(a)]. Especially, stroke survivors had more difficulty in reaching extended position [the right-half-plane of the workspace in Fig. 6(a)] than curled position. The reduced workspace for different patients may be due to different changes at the individual joints: for subject S3, who had almost no control of wrist movement, the difficulty seemed mostly due to the restricted wrist movement [Fig. 6(b) and (d)]; for others (S1 and S2), the difficulty seemed due to the combination of all three joints (i.e., shoulder, elbow, and wrist) [Fig. 6(b)–(d)].

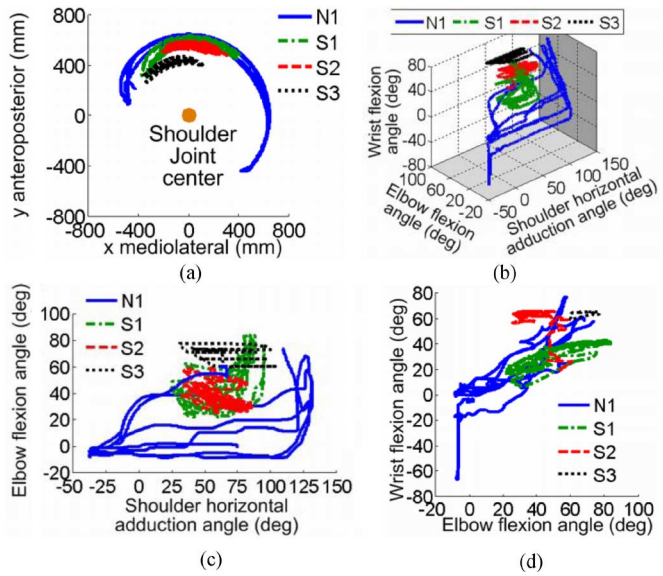

Fig. 6. Active workspace in the arm extension directions: (a) workspace of hand in the horizontal (transverse) plane with origin corresponding to shoulder joint center; (b) corresponding shoulder, elbow, and wrist joint angles in 3-D joint space; (c) projection of (b) onto shoulder-elbow-joint-angle plane [light-grey horizontal plane of (b)]; and (d) projection of (b) onto elbow-wrist-joint-angle plane [dark-grey side plane of (b)]. Compared with the healthy control (N1; blue solid line), stroke survivors (S1, S2, S3) demonstrated reduced active workspace.

Based on the diagnosis, the different patterns of abnormal couplings could potentially be treated on an impairment-specific basis in the subsequent passive stretching and (assistive/resistive) active movement therapy.

C. Evaluation of Stretching and Movement Training Induced Changes at the Shoulder, Elbow, and Wrist

The spastic arm/joints of stroke survivors were stretched by using the ISS described in Section II-C. On one hand, shoulder, elbow, or wrist of the hypertonic and impaired arm was stretched individually, focusing on the joints/DOFs with increased individual joint/DOF stiffness identified by the robot-aided diagnosis given in Section III-B. On the other hand, simultaneous shoulder, elbow and wrist stretching was carried out to loosen the stiff muscles-joints of stroke survivors, reducing excessive couplings across the joints/DOFs as well as individual joint/DOF stiffness.

As representative results following strenuous and safe passive stretching of the shoulder, elbow, and wrist joints for about 40 min, movement ROM of the (impaired) arm of the stroke survivors increased considerably, especially near the extended arm position (Table I). Further, individual joint/DOF stiffness of all three joints (Table II) of stroke survivors was reduced. Subjectively, the stroke survivors felt the passive stretching loosened their stiff arms. The excessive couplings across the joints/DOFs were also reduced after the stretching. For example, cross-coupled stiffness between joints/DOFs (Table III) was reduced after stretching. Especially, at the end of shoulder H.Add PROM, 50% reduction was observed in cross-coupled stiffness relating

elbow CT and shoulder H.Add angle. Moreover, elbow maximum CT was reduced considerably in both directions. Before stretching, the maximum elbow CTs were 0.57 ± 0.15 Nm in Ex and 1.37 ± 0.19 Nm in Fl, and reduced to 0.55 ± 0.26 Nm in Ex and 1.04 ± 0.32 Nm in Fl, after stretching.

IV. Discussion and Conclusion

An upper limb exoskeleton neurorehabilitation robot, the IntelliArm, was developed, aiming to support clinicians and patients in all four steps of neurorehabilitation (Fig. 1) with the following novel integrated capabilities: 1) quantitative, objective and comprehensive MJMD *pre-evaluation capabilities aiding diagnosis* (e.g., single and cross-joint evaluation of PROM and stiffness in passive movement, and loss of individuation in active movement) for individual patients; 2) strenuous and safe *passive stretching* of hypertonic/deformed arm for loosening muscles/joints based on the robot-aided diagnosis; 3) *(assistive/resistive) active reaching training* after passive stretching for regaining/improving motor control ability; and 4) quantitative, objective, and comprehensive *outcome evaluation* at the level of individual joints/DOFs, multiple joints/DOFs, and whole arm.

The IntelliArm's MJMD evaluation capabilities aiding diagnosis can provide valuable information on 1) which joints and which DOFs have significant changes in the neuromechanical properties; 2) which joints lose independent control [e.g., loss of individuation with NRMDS, which may have a potential correlation with MSS (Fig. 5)]; 3) what are the abnormal couplings; and 4) whether the impairment is due to deficits in passive muscle properties or active control capabilities (e.g., much higher elbow coupling torque during active shoulder H.Abd than that during passive shoulder H.Abd). Thus, the clinicians can make more informed decision on the type, intensity, and duration of therapy of each patient. Moreover, the prescribed type, intensity, and duration of therapy can be realized with the same robot by utilizing its passive stretching and (assistive/resistive) active movement training capabilities. Further, the outcome of the therapy can also be evaluated with the same robot in a consistent manner. In short, the IntelliArm may possibly be used for all steps of neurorehabilitation seamlessly as a convenient tool.

An extension of this research would be to test its integrated capabilities with more patients with neurological disorders to corroborate its effectiveness and efficacy, and to validate reliability of the measurement procedure.

Acknowledgment

L.-Q. Zhang and Y. Ren have equity positions in Rehabtek LLC, which is involved in developing the IntelliArm in this study.

References

[1] L.-Q. Zhang and W. Z. Rymer, "Simultaneous and nonlinear identification of mechanical and reflex properties of human elbow joint muscles," *IEEE Trans. Biomed. Eng.*, vol. 44, no. 12, pp. 1192–1209, Dec. 1997.

[2] T. Nef, M. Mihelj, and R. Riener, "ARMin: A robot for patient-cooperative arm therapy," *Med. Biol. Eng. Comput.*, vol. 45, pp. 887–900, 2007.

[3] T. Nef, M. Guidali, and R. Riener, "ARMin III—Arm therapy exoskeleton with an ergonomic shoulder actuation," *Appl. Bionics. Biomech.*, vol. 6, pp. 127–142, 2009.

[4] C. G. Burgar, P. S. Lum, P. C. Shor, and H. F. M. Van der Loos, "Development of robots for rehabilitation therapy: The Palo Alto VA/stanford experience," *J. Rehabil. Res. Develop.*, vol. 37, pp. 663–673, 2000.

[5] J. J. Palazzolo, M. Ferraro, H. I. Krebs, D. Lynch, B. T. Volpe, and N. Hogan, "Stochastic estimation of arm mechanical impedance during robotic stroke rehabilitation," *IEEE Trans. Neural. Syst. Rehabil. Eng.*, vol. 15, no. 1, pp. 94–103, Mar. 2007.

[6] P. H. Chang and S. H. Kang, "Stochastic estimation of human arm impedance under nonlinear friction in robot joints: A model study," *J. Neurosci. Methods*, vol. 189, pp. 97–112, 2010.

[7] P. H. Chang, K. Park, S. H. Kang, H. I. Krebs, and N. Hogan, "Stochastic estimation of human arm impedance using robots with nonlinear frictions: An experimental validation," *IEEE/ASME Trans. Mechatron.*, vol. 18, no. 2, pp. 775–786, Apr. 2013.

[8] S. H. Kang and L.-Q. Zhang, "Robust identification of multi-joint human arm impedance based on dynamics decomposition: A modeling study," in *Proc. 33rd Annu. Int. Conf. IEEE Eng. Med. Biol. Soc.*, Boston, MA, 2011, pp. 4453–4456.

[9] D. J. Reinkensmeyer, J. P. Dewald, and W. Z. Rymer, "Guidance-based quantification of arm impairment following brain injury: A pilot study," *IEEE Trans. Rehabil. Eng.*, vol. 7, pp. 1–11, Mar. 1999.

[10] H. I. Krebs, N. Hogan, M. L. Aisen, and B. T. Volpe, "Robot-aided neurorehabilitation," *IEEE Trans. Rehabil. Eng.*, vol. 6, no. 1, pp. 75–87, Mar. 1998.

[11] J. P. A. Dewald, P. S. Pope, J. D. Given, T. S. Buchanan, and W. Z. Rymer, "Abnormal muscle coactivation patterns during isometric torque generation at the elbow and shoulder in hemiparetic subjects," *Brain*, vol. 118, pp. 495–510, 1995.

[12] M. Ellis, A. Acosta, J. Yao, and J. Dewald, "Position-dependent torque coupling and associated muscle activation in the hemiparetic upper extremity," *Exp. Brain Res.*, vol. 176, pp. 594–602, 2007.

[13] A. Shumway-Cook and M. H. Woollacott, *Motor Control: Theory and Practical Applications*, 2nd ed. Philadelphia, PA: Lippincott Williams Wilkins, 2001, ch. 6.

[14] K. M. Zackowski, A. W. Dromerick, S. A. Sahrmann, W. T. Thach, and A. J. Bastian, "How do strength, sensation, spasticity and joint individuation relate to the reaching deficits of people with chronic hemiparesis?," *Brain*, vol. 127, pp. 1035–1046, 2004.

[15] N. H. Mayer, A. Esquenazi, and M. K. Childers, "Common patterns of clinical motor dysfunction," *Muscle Nerve*, vol. 6, pp. S21–S35, 1997.

[16] L.-Q. Zhang, S. G. Chung, Z. Bai, E. M. van Rey, M. W. Rogers, M. E. Johnson, and E. J. Roth, "Intelligent stretching for ankle joints with contracture/spasticity," *IEEE Trans. Neural. Syst. Rehabil. Eng.*, vol. 10, no. 3, pp. 149–157, Sep. 2002.

[17] R. W. Selles, X. Li, F. Lin, S. G. Chung, E. J. Roth, and L.-Q. Zhang, "Feedback-controlled and programmed stretching of the ankle plantarflexors and dorsiflexors in stroke: Effects of a 4-week intervention program," *Arch. Phys. Med. Rehabil.*, vol. 86, pp. 2330–2336, 2005.

[18] D. Lynch, M. Ferraro, J. Krol, C. M. Trudell, P. Christos, and B. T. Volpe, "Continuous passive motion improves shoulder joint integrity following stroke," *Clin. Rehabil.*, vol. 19, pp. 594–599, 2005.

[19] F. Gao, Y. Ren, E. J. Roth, R. Harvey, and L.-Q. Zhang, "Effects of repeated ankle stretching on calf muscle—Tendon and ankle biomechanical properties in stroke survivors," *Clin. Biomech.*, vol. 26, pp. 516–522, 2011.

[20] Y.-N. Wu, M. Hwang, Y. Ren, D. Gaebler-Spira, and L.-Q. Zhang, "Combined passive stretching and active movement rehabilitation of lower-limb impairments in children with cerebral palsy using a portable robot," *Neurorehab. Neural Repair*, vol. 25, pp. 378–385, 2011.

[21] F. Gao and L.-Q. Zhang, "Altered contractile properties of the gastrocnemius muscle poststroke," *J. Appl. Physiol.*, vol. 105, pp. 1802–1808, 2008.

[22] R. Riener, T. Nef, and G. Colombo, "Robot-aided neurorehabilitation of the upper extremities," *Med. Biol. Eng. Comput.*, vol. 43, pp. 2–10, 2005.

[23] S. G. Chung, E. M. van Rey, Z. Bai, E. J. Roth, and L.-Q. Zhang, "Biomechanic changes in passive properties of hemiplegic ankles with spastic hypertonia," *Arch. Phys. Med. Rehabil.*, vol. 85, pp. 1638–1646, 2004.

[24] S. G. Chung, E. van Rey, Z. Bai, W. Z. Rymer, E. J. Roth, and L.-Q. Zhang, "Separate quantification of reflex and nonreflex components of spastic hypertonia in chronic hemiparesis," *Arch. Phys. Med. Rehabil.*, vol. 89, pp. 700–710, 2008.
[25] C. Bosecker, L. Dipietro, B. Volpe, and H. I. Krebs, "Kinematic robot-based evaluation scales and clinical counterparts to measure upper limb motor performance in patients with chronic stroke," *Neurorehabil. Neural Repair*, vol. 24, pp. 62–69, 2010.
[26] R. Loureiro, F. Amirabdollahian, M. Topping, B. Driessen, and W. Harwin, "Upper limb robot mediated stroke therapy—GENTLE/s approach," *Auton. Robot.*, vol. 15, pp. 35–51, 2003.
[27] G. Prange, M. Jannink, C. Groothuis-Oudshoorn, H. Hermens, and M. Ijzerman, "Systematic review of the effect of robot-aided therapy on recovery of the hemiparetic arm after stroke," *J. Rehabil. Res. Dev.*, vol. 43, pp. 171–184, 2006.
[28] B. Brewer, S. McDowell, and L. Worthen-Chaudhari, "Poststroke upper extremity rehabilitation: A review of robotic systems and clinical results," *Top Stroke Rehabil.*, vol. 14, pp. 22–44, 2007.
[29] S. H. Kang, M. Jin, and P. H. Chang, "A solution to the accuracy/robustness dilemma in impedance control," *IEEE/ASME Trans. Mechatron.*, vol. 14, no. 3, pp. 282–294, Jun. 2009.
[30] S. H. Kang, "Robust IMC based impedance control of robot manipulators," Ph.D. dissertation, Dept. Mech. Eng., KAIST, Daejeon, Republic Korea, 2009.
[31] M. Domalain, L. Vigouroux, and E. Berton, "Determination of passive moment-angle relationships at the trapeziometacarpal joint," *J. Biomech. Eng.*, vol. 132, pp. 2628–2635, 2010.
[32] Y. S. Yoon and J. M. Mansour, "The passive elastic moment at the hip," *J. Biomech.*, vol. 15, pp. 905–910, 1982.
[33] R. Riener and T. Edrich, "Identification of passive elastic joint moments in the lower extremities," *J. Biomech.*, vol. 32, pp. 539–544, 1999.
[34] P. D. Hoang, R. B. Gorman, G. Todd, S. C. Gandevia, and R. D. Herbert, "A new method for measuring passive length—Tension properties of human gastrocnemius muscle in vivo," *J. Biomech.*, vol. 38, pp. 1333–1341, 2005.
[35] H. Zhao, Y.-N. Wu, M. Hwang, Y. Ren, F. Gao, D. Gaebler-Spira, and L.-Q. Zhang, "Changes of calf muscle-tendon biomechanical properties induced by passive-stretching and active-movement training in children with cerebral palsy," *J. Appl. Physiol.*, vol. 111, pp. 435–442, 2011.
[36] M. Ferraro, J. H. Demaio, J. Krol, C. Trudell, K. Rannekleiv, L. Edelstein, P. Christos, M. Aisen, J. England, S. Fasoli, H. Krebs, N. Hogan, and B. T. Volpe, "Assessing the motor status score: A scale for the evaluation of upper limb motor outcomes in patients after stroke," *Neurorehabil. Neural Repair*, vol. 16, pp. 283–289, 2002.

Yupeng Ren (SM'11) received the B.S. degree in mechanical engineering and the M.S. degree in biomedical engineering from Tsinghua University, Beijing, China, in 2001 and 2004, respectively.

In 2005, he joined Sensory Motor Performance Program (SMPP), Rehabilitation Institute of Chicago (RIC), Chicago, IL, USA, where he is currently a Research Associate. He is also a R&D Engineer and conducts Small Business Innovation Research (SBIR) programs at Rehabtek LLC, Wilmette, IL, USA. His research and development interests include robot-assisted technology, rehabilitation robot application for stroke survivors and children with cerebral palsy, and home-based robot solutions.

Sang Hoon Kang (M'12) received the B.S., M.S., and Ph.D. degrees in mechanical engineering from Korea Advanced Institute of Science and Technology (KAIST), Daejeon, Korea, in 2000, 2002, and 2009, respectively.

In 2010, he joined SMPP, RIC, where he is currently a Research Associate. He is also a Postdoctoral Research Fellow at the Department of Physical Medicine and Rehabilitation, and an Instructor at the Department of Biomedical Engineering, Northwestern University, Chicago, IL, USA. His current research interests include rehabilitation robotics and biomechanics of human movement with emphasis on rehabilitation medicine.

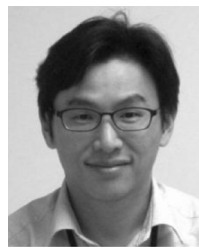

Hyung-Soon Park (M'05) received the Ph.D. degree in mechanical engineering from Korea Advanced Institute of Science and Technology (KAIST), Daejeon, Korea, in 2004.

He is a staff scientist in the Rehabilitation Medicine Department, Clinical Center at the National Institutes of Health, Bethesda, MD. His current research interest focuses mainly on application of robotics and control technology on rehabilitation medicine, and biomechanics of human movement.

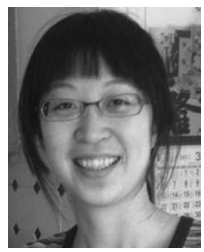

Yi-Ning Wu received B.S. degree in physical therapy and the Ph.D. degree in biomedical engineering from National Cheng Kung University, Tainan, Taiwan, in 2000 and 2007, respectively.

She is currently a Research Associate in the Neuroscience Department in Brown University and Brown Institute for Brain Science. Her research interests include the rehabilitative technology in children and adults with brain injury, neuroplasticity, and motor behavior.

Li-Qun Zhang (SM'06) received the B.E. degree in electrical engineering from Tsinghua University, Beijing, China, in 1982, and the M.S. and Ph.D. degrees in biomedical engineering from Vanderbilt University, Nashville, TN, USA, in 1988 and 1990, respectively.

Since 1991, he has been at the RIC and Northwestern University, Chicago, IL, USA, where he is currently a Senior Research Scientist, Raisbeck Professor of Orthopaedic Surgery, and Professor. His research interests include development of intelligent rehabilitation devices to perform diagnosis, passive stretching and active movement treatments, and outcome evaluations of impaired limbs in stroke, investigation of reflex and nonreflex factors contributing to limb impairments at the multi- and single-joint and muscle fascicle/fiber levels, and investigation of musculoskeletal injury mechanisms and rehabilitation and prevention of the injuries.